

Electrically Induced Conformational Change of Peptides on Metallic Nanosurfaces

Yi Chen,^{†,‡,§} Eduardo R. Cruz-Chu,^{§,⊥,¶} Jaie C. Woodard,[⊥] Manas R. Gartia,^{†,||} Klaus Schulten,^{§,⊥,Δ,*} and Logan Liu^{†,‡,*}

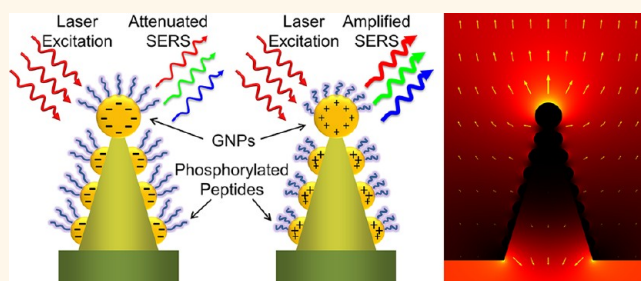
[†]Micro and Nanotechnology Laboratory, University of Illinois at Urbana—Champaign, [‡]Department of Electrical and Computer Engineering, University of Illinois at Urbana—Champaign, [§]Center for Biophysics and Computational Biology, University of Illinois at Urbana—Champaign, [⊥]Beckman Institute for Advanced Science and Technology, University of Illinois at Urbana—Champaign, ^{||}Department of Nuclear, Plasma and Radiological Engineering, University of Illinois at Urbana—Champaign, and ^ΔDepartment of Physics, University of Illinois at Urbana—Champaign, Urbana, Illinois 61801, United States. *These authors contributed equally to this study.

The responses of biomolecules to external stimuli are the focus of many studies and applications in biomedicine. Physical stimuli, such as mechanical,¹ thermal,² optical,³ and electrical ones,⁴ alter and manipulate energy, composition, structure, and conformation and, thus, change and control function and activity of biomolecules. For example, molecular switches can be reversibly shifted between two or more stable states in response to external stimuli, such as force,⁵ temperature,⁶ light,⁷ and electrical potential.⁸ Most of the manipulations, especially mechanical and electrical ones, are mediated by a molecule—solid interface.^{1,4,5,7,8}

Biological and chemical stimuli, such as pH variation,⁹ microenvironment change,¹⁰ and the presence or absence of a ligand,¹¹ can also induce compositional and structural changes to molecules in a biomimetic system, such that these molecules can act as sensors^{12,13} as long as the intermolecular or intramolecular effects can be detected and reported. On the basis of this idea, various lab-on-a-chip devices¹⁴ have been created, such as DNA,¹⁵ protein,¹⁶ and antibody¹⁷ microarrays, and numerous spectroscopic techniques have been adopted, such as fluorescence,¹⁸ vibrational,¹⁹ and nuclear magnetic resonance,²⁰ to detect and monitor the conformational change in biomolecules.

In the present study, we employ surface-tethered peptide probes for kinase enzymes to demonstrate in an exemplary fashion electrical manipulation and spectroscopic detection of intramolecular conformational change in the sub-nanometer range possible today. The function of kinases is to activate other proteins through phosphorylation, *i.e.*,

ABSTRACT



Surface immobilized biomolecular probes are used in many areas of biomedical research, such as genomics, proteomics, immunology, and pathology. Although the structural conformations of small DNA and peptide molecules in free solution are well studied both theoretically and experimentally, the conformation of small biomolecules bound on surfaces, especially under the influence of external electric fields, is poorly understood. Using a combination of molecular dynamics simulation and surface-enhanced Raman spectroscopy, we study the external electric field-induced conformational change of dodecapeptide probes tethered to a nanostructured metallic surface. Surface-tethered peptides with and without phosphorylated tyrosine residues are compared to show that peptide conformational change under electric field is sensitive to biochemical modification. Our study proposes a highly sensitive *in vitro* nanoscale electro-optical detection and manipulation method for biomolecule conformation and charge at bio—nano interfaces.

KEYWORDS: electrically induced conformational change · molecule—gold interface · gold nanoparticle · surface-enhanced Raman spectroscopy · molecular dynamics

through transfer of a phosphate group (PO_3^{2-}) from ATP to proteins, usually on serine, threonine, or tyrosine residues. Disruptions of kinase signaling pathways are frequent causes for diseases, such as cancer and diabetes.²¹ The various conformations of peptide probes with or without phosphorylation arise from the charges of the ionized phosphate groups added by kinases

* Address correspondence to loganliu@illinois.edu; kschulte@ks.uiuc.edu.

Received for review June 20, 2012 and accepted August 16, 2012.

Published online August 16, 2012
10.1021/nn3027408

© 2012 American Chemical Society

as well as from the interaction with the charges on the nanostructured surface material. If an electric field is applied across the peptide probes, either phosphorylated or not, the probe's conformation will be altered due to the electrostatic force and the structural difference between a peptide probe with and without a phosphate group will be amplified. In particular, the relative distance between the phosphorylated residue in the peptide probe and the nanostructured surface material will be influenced significantly. In our study, this distance change is detected by a near-field optical detection method, surface-enhanced Raman spectroscopy (SERS), in which the signal intensity is inversely proportional to the 12th power of the distance between chemical analyte and nanostructured metallic surface.²² To elucidate the actual conformational changes that occur, and to interpret the experimental findings, molecular dynamics (MD) simulations are carried out to visualize the structural dynamics of the attached peptide probes. Through the combined effort of experiments and simulations, we study the details of peptide conformational change on nanostructure surfaces as well as propose a highly sensitive sensor for detecting changes in molecular conformation.

RESULTS AND DISCUSSION

In a previous study,²³ it was shown that a Schottky junction can be formed between adsorbed molecules and a metal surface. The underlying near-field interaction not only is a likely contributing factor for SERS but also modifies the charge distribution of attached molecules. In free solution, charge distribution and conformation of molecules are determined by the ion species and pH value of a buffer solution; however, the strong charge interaction between molecules and a metallic surface²⁴ provides a route to control the conformation of the molecules by changing the charge distribution of the metallic surface, which is achievable through application of an electric potential. Here, we employ a synthetic peptide sequence and its phosphorylated counterpart as exemplary small molecules as well as a gold surface connected to a dc power source (Figure 1a).

The peptide sequence employed (EGIYGVLFKKCC) is a commercially available kinase profiling peptide substrate.²⁵ The oligopeptide contains a tyrosine at position 4, a target for phosphorylation by Src kinase (Figure 1b). The N-terminus is labeled with rhodamine 6G (*rho*) to permit a spectroscopic response. The C-terminus includes a cysteine used to attach the peptide to the gold surface through a gold–thiol bond (see Methods). The gold surface, as the bottom electrode, is connected with an indium tin oxide (ITO) top electrode through a dc power source to form a parallel-plate capacitor. By applying a dc voltage to the capacitor, the gold surface is biased positively or negatively

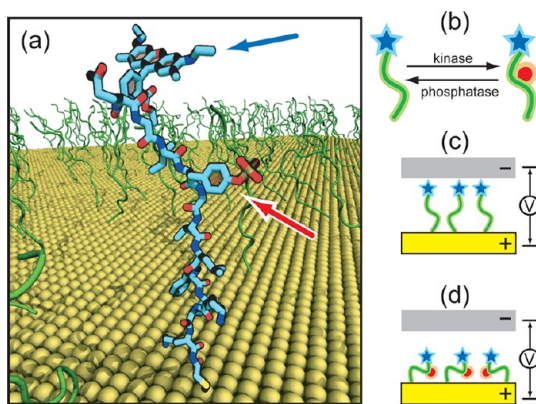


Figure 1. Electrical control of molecular conformations through a charged metal surface. (a) Highlighted in the front is an atomic model of the peptide-*rho* system tethered to the gold surface colored in yellow. This surface is assumed to be planar at the $10.2 \text{ nm} \times 10.2 \text{ nm}$ scale simulated. Other peptide probes are colored in green. The front peptide is highlighted in licorice representation; carbon atoms are colored in light blue, nitrogen atoms dark blue, oxygen atoms red, and phosphate atoms yellow; for the sake of clarity hydrogen atoms are not shown; blue and red arrows point to the *rho* cap and the phosphorylated tyrosine residue, respectively. (b) Kinases or phosphatases add or remove a phosphate group to (on) the peptide probes and thus modify the net charge of the probes. The peptide is represented as a green line, the phosphate group as a red dot, and the *rho* fluorescence probe as a blue star. (c) Non-phosphorylated peptides are nearly neutral and unaffected by charges on the metal surface. (d) Phosphorylation introduces a net charge of $-2e$ to the peptides, which leads to bending of the peptides under positive surface charge polarity.

with measurable charge densities (Figure 1c,d). The non-phosphorylated sequence used here is nearly neutral in buffer solution. Phosphorylation of peptides with isoelectric point $pI > 7.0$ usually results in a large shift of pI to lower values,²⁶ and in the present case, the phosphate group added to the tyrosine at position 4 introduces a net negative charge of $-2e$; therefore, the peptide conformation becomes responsive to the surface charge. On a positively charged metal surface with electric field pointing toward the top ITO electrode, the non-phosphorylated peptides experience minimal conformation change (Figure 1c), while the phosphorylated ones bend toward the gold surface (Figure 1d).

The conformational changes mentioned above can be experimentally detected *in situ* by monitoring SERS signal changes under different electric fields. The distance change between the free end of the peptide and the gold surface, reflecting peptide stretching or coiling, can also be captured from the different measured SERS signal intensities. To enhance this spectroscopic signal, we employ a high-quality gold-coated SERS substrate as shown in the schematic drawing and SEM image (Figure 2a,b). This device is a high-density silicon nanocone array coated with gold nanoparticles (GNPs). The silicon nanocone array is fabricated by a simultaneous bottom-up and top-down process

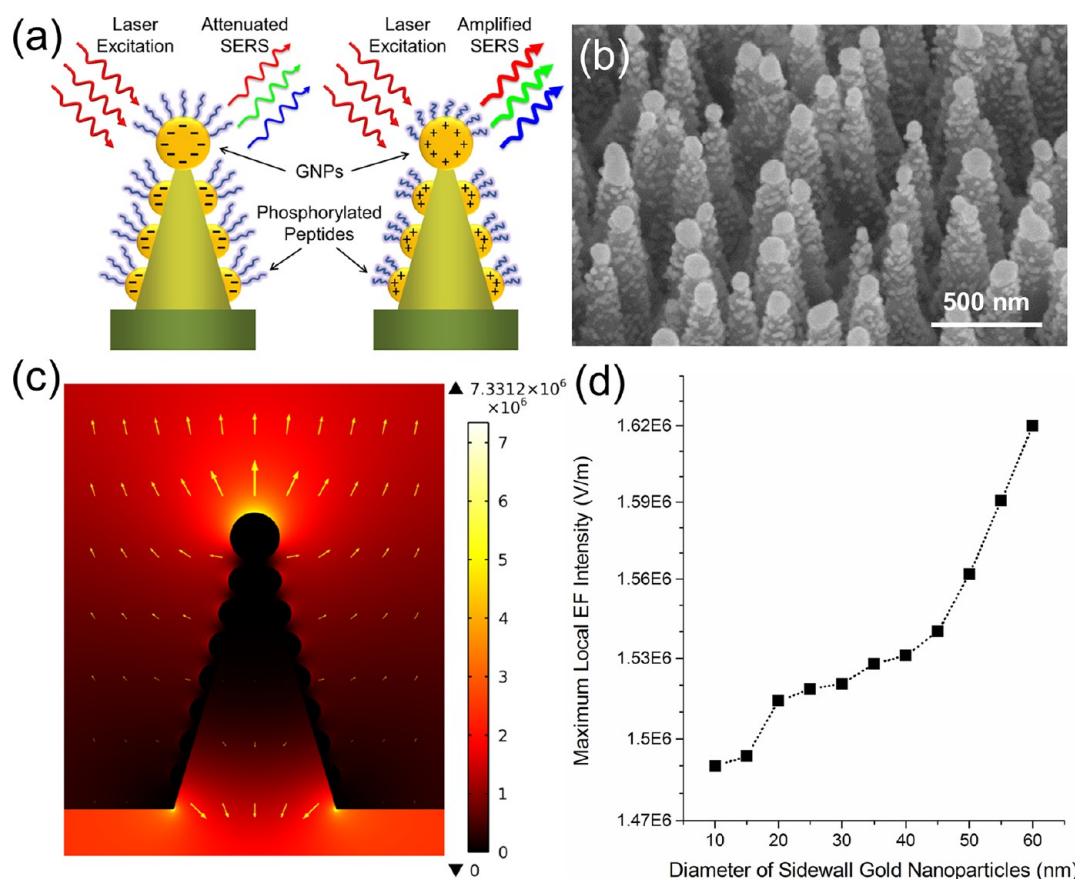


Figure 2. Topology of experimental nanodevice. (a) Schematic drawing of GNP-coated nanocones and surface-tethered peptides. GNP are colored in yellow; peptides in blue. SERS signals are attenuated or amplified when peptides stretch or coil under different surface charge polarities. (b) Scanning electron microscope image showing silicon nanocone array with uniformly coated GNP at the tips and sidewalls. (c) Calculated enhancement of electrostatic field near a GNP-coated silicon nanocone surface. The GNPs on the top and sidewall of the nanocone are 90 and 50 nm in diameter, respectively. The top electrode is $1.5 \mu\text{m}$ away from the bottom surface. The electric field near the GNP surface reveals a high-field gradient near the tethered peptides. The maximum field strength is $7.33 \times 10^6 \text{ V m}^{-1}$ and arises near the top of the nanocones. The yellow arrows represent the electric field directions and strength. (d) The dependence of the maximum local electrical field intensity near the sidewall GNP surface on the diameter of GNPs. The results show stronger localized electrical field for larger GNPs.

discussed in a previous publication.²⁷ The GNPs are created by an e-beam evaporation process. Due to the large slope of the sidewall ($>75^\circ$), instead of forming a uniform layer of gold film, the deposition of gold on the silicon nanocone surface follows a kind of Volmer–Weber growth, forming isolated nanoparticles of around 50 nm in diameter.²⁸ The GNPs on the nanocone surface form two types of nanogaps: (i) inter-nanoparticle gaps on single nanocones and (ii) inter-nanocone gaps between nanoparticles on adjacent nanocones. Thus, compared with conventional two-dimensional metallic nanoparticle arrays, the present device has a much higher SERS hot-spot density, resulting in much higher SERS sensitivity. In a previous study,²⁹ we have demonstrated similar substrates with an enhancement factor of 10^8 – 10^9 to Raman signals.

Figure 2a illustrates our phosphorylated peptide–GNP conjugation system at the nanoscale. An enhanced localized electrostatic field pointing in two opposite directions can be formed by cumulated negative or positive charges on each individual GNP

surface (Figure 2c). The strength of the electrostatic field can be controlled by changing the size of the GNPs (Figure 2d). The electric field component orthogonal to the gold surface induces, depending on sign, stretching or coiling of the phosphorylated peptides (Figure 2a), which attenuates or amplifies the SERS signal following the aforementioned 12th power law. Conversely, non-phosphorylated peptides carrying no extra charge should contribute with a constant, namely, field-insensitive Raman scattering signal.

In order to visualize the molecular processes on the SERS substrate surface at the atomic scale, we carried out molecular dynamics simulations as described in Methods, employing the simulations as a computational microscope.³⁰ In a MD simulation system of a 5×5 peptide array on a $10.2 \text{ nm} \times 10.2 \text{ nm}$ area, the gold surface is assumed to be planar, as shown in Figure 1a. The MD simulations clearly revealed that conformational changes of a single peptide are induced by external electric fields, providing theoretical support for the mechanism discussed above, as well as offering

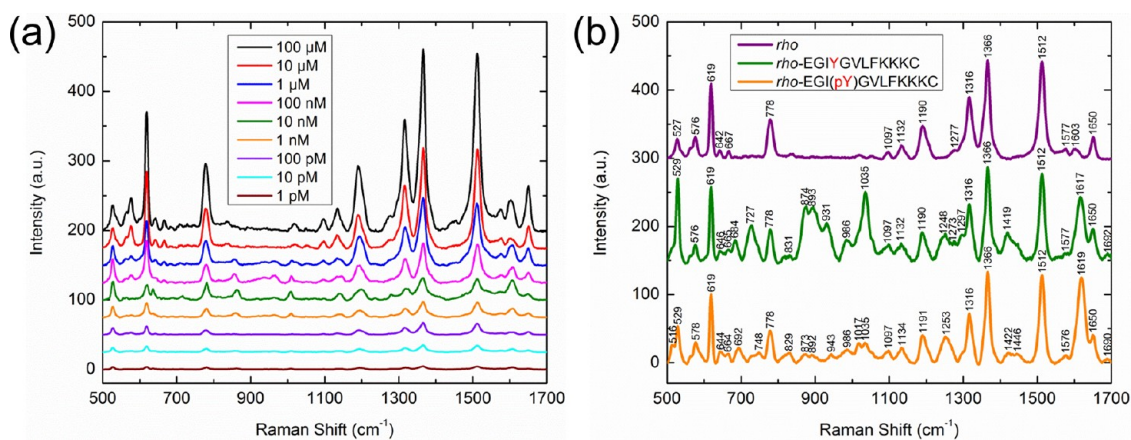


Figure 3. SERS sensitivity for phosphorylation detection. (a) Representative SERS spectra of serially diluted *rho* solutions spotting on the substrate surface. Concentrations from 100 μ M down to 1 pM were faithfully detected, displaying a sensitivity down to 1 part per billion. (b) Comparison of SERS spectra for *rho*, *rho*-labeled non-phosphorylated, and *rho*-labeled phosphorylated peptide sequences, all in aqueous solution. SERS peaks are labeled by corresponding wave numbers; the latter are assigned to specific vibrations in Table S1 in the Supporting Information. The spectra are equally offset in the plot in order to display all spectra clearly.

explanations for the spectroscopic data presented below.

We first tested the Raman profiling capacity of the SERS substrate (see Methods for instrumentation; see Supporting Information for experimental setup). We found that Raman signals of *rho* molecules and surface-tethered peptides, indeed, were greatly amplified, easily detectable, and unambiguously discernible (Figure 3). Figure 3a shows the representative SERS spectra of *rho* molecules at different concentrations, corresponding to the molecular monolayers with different surface coverage ratios. The relative intensities of SERS signals decreased linearly with serially diluted *rho* solutions;³¹ however the primary Raman peak signature of *rho* was still clearly identifiable at a concentration as low as 1 pM (1 part per billion) level, indicating the ultrahigh sensitivity of the SERS substrate. This prompted us to test whether the substrate is sensitive enough to distinguish the *rho* molecules, *rho*-labeled phosphorylated peptides (*rho*-EGI(pY)-GVLFKFKC), and *rho*-labeled non-phosphorylated peptides (*rho*-EGI(Y)GVLFKFKC). As seen in Figure 3b, compared with the spectrum of *rho* molecules, some additional Raman peaks appeared in the peptide SERS spectra. We also found that specificity and magnitude of SERS signals were significantly altered between the phosphorylated and non-phosphorylated states (see Supporting Information for band assignments and analysis). Other peptide sequences, including ones previously used in tyrosine-kinase assays (IYGEFKKAAC)³² or known as regulatory sites of oncogenic Src kinases (IEDNEYTARQGGC), were tested and reported in previous work.^{33,34} Altogether, the experiments confirmed that our substrate is sensitive enough to capture a SERS signal difference due to a change in peptide phosphorylation state.

As illustrated in Figure 1c,d, application of an electric field orthogonal to the nanochip should bend the

peptides toward the gold surface or stretch them away from it. Due to the charge²⁴ or electromagnetic³⁵ coupling effect, the SERS signal is very sensitive to the distance between peptides and the gold surface,²² and a significant SERS variation is expected for even a slight conformational change. The averaged SERS spectra for non-phosphorylated and phosphorylated peptides are shown in Figure 4a and b, respectively. The spectra were measured under 0, ± 1.2 V conditions. For the non-phosphorylated peptide probe, the SERS signal intensity did not register an observable change under different voltage conditions; however, for the phosphorylated peptide probe, the SERS signal intensity exhibited a significant change, namely, a higher signal for positive electric field and a lower one for negative electric field. The standard deviation around the mean (area plot under SERS spectra) is less than 10%, demonstrating the systematic character of conformational changes under electric field conditions.

The averaged SERS spectra under 0, ± 1.2 V conditions are shown color-coded at the top of Figure 4c and d for non-phosphorylated peptides and phosphorylated peptides, respectively. The color coding allows rapid visual assertion of similarities and/or differences of SERS signals in side-by-side comparison. As one can see in Figure 4c, in the case of non-phosphorylated peptides, the three spectra are extremely similar in peak (red) and valley (green) locations and intensities. However, in Figure 4d, a clear difference in the color pattern can be discerned in the case of phosphorylated peptides with a mostly red (high intensity for +1.2 V) and green (low intensity for -1.2 V) SERS profile. The similarities and/or differences can be further confirmed by calculating the Log₂-fold variation of the SERS signal at ± 1.2 V relative to the original 0 V state, as can be seen in the bottom two lanes of Figure 4c,d. For non-phosphorylated peptides, the variations are

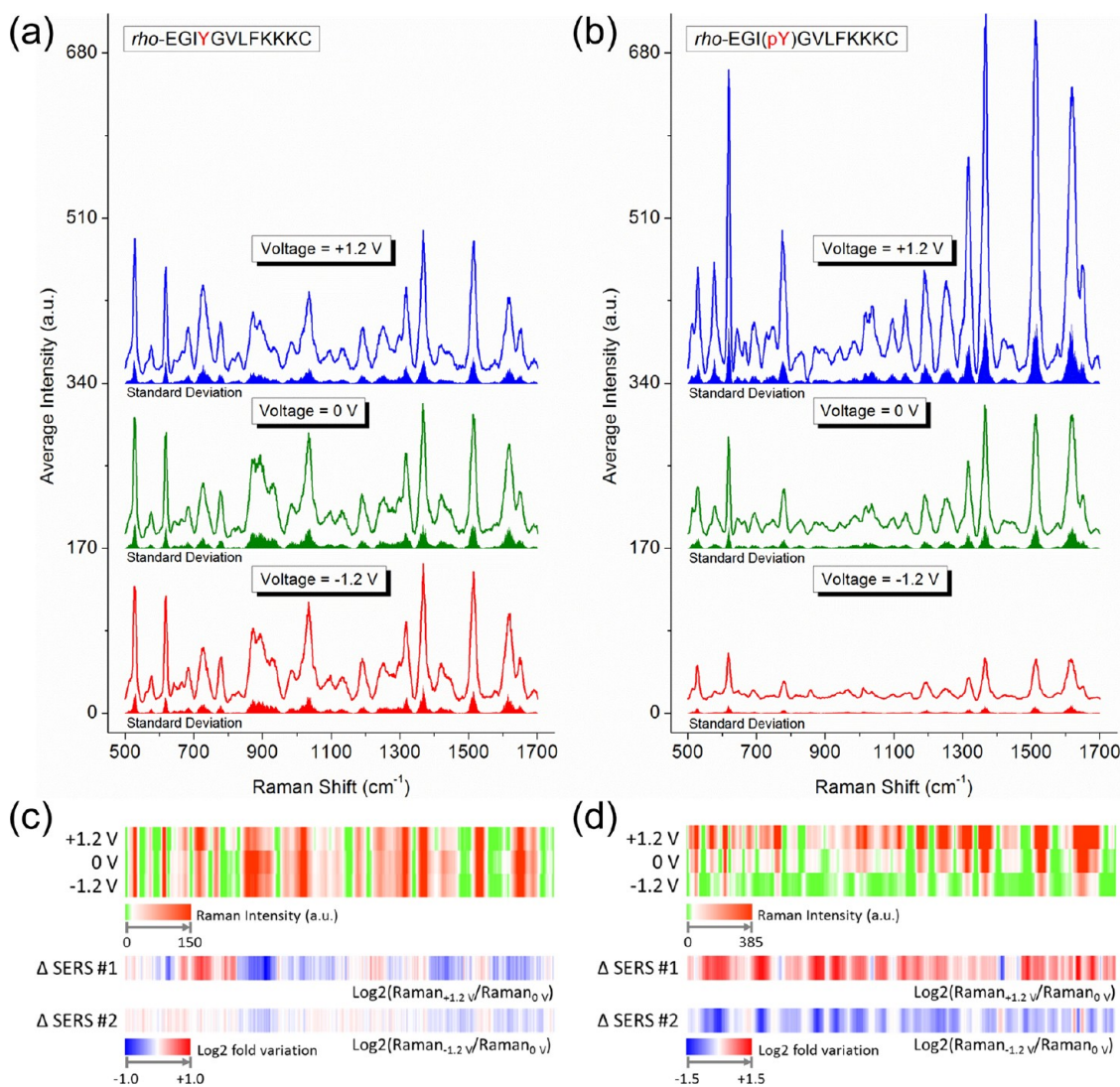


Figure 4. SERS spectra and statistical analysis of peptide probes for different voltages. (a, b) Averaged raw SERS spectra and standard deviation (area plot below each spectrum) of non-phosphorylated (a) and phosphorylated (b) peptide probes under 0, ± 1.2 V bias. The spectra are equally offset in the plot in order to display all spectra clearly. (c, d) Color-coded mean SERS spectra of non-phosphorylated (c) and phosphorylated (d) peptide probes under 0, ± 1.2 V bias (top three lanes) along with the Log₂-fold variations of SERS spectra intensity with and without applied electric field (bottom two lanes). In (a) and (b), Raman shift is represented linearly in the range 500 to 1700 cm^{-1} . Raman signal intensity and Log₂-fold variations are represented by a color scale ranging from green to red (0–150 (c) and 0–385 (d)) and from blue to red (–1.0 to +1.0 (c) and –1.5 to +1.5 (d)), respectively, as shown by color bars (in units of standard deviation shown in a, b).

within $\pm\sigma$ (standard deviation) bounds, actually close to 0 at most Raman shifts. In contrast, for phosphorylated peptides the Log₂-fold variations under +1.2 V are close to $+1.5\sigma$ (red color) at most Raman shifts, and those under –1.2 V electric field are close to -1.5σ (blue color).

The above results demonstrate that the presence or absence of phosphate groups on peptide probes is easily identified spectroscopically on the metallic nanosurface through SERS signal amplification or attenuation. MD simulations were performed to validate the interpretation of SERS signals at atomic resolution. However, such simulations suffer from a limitation in the accessible time scale. Current simulations cover typically only hundreds of nanoseconds,

which is not long enough to explore low voltage-induced bending/stretching of peptides. To circumvent this problem and speed up the molecular responses, high-voltage biases were employed (the issue is discussed further below). In the simulations we also chose to describe the gold surface to which the peptides were tethered as planar, while it actually has some degree of curvature (Figure 2). On the scale of the 10.2 nm \times 10.2 nm area simulated, it is reasonable to assume a planar surface considering the much larger size (50 nm) of a single GNP (Figure 2b). Other limitations intrinsic to our MD simulations are force field quality and system size simulated.^{36,37} Even though the outcome of MD studies is affected by those limitations, the MD simulations carried out should provide a

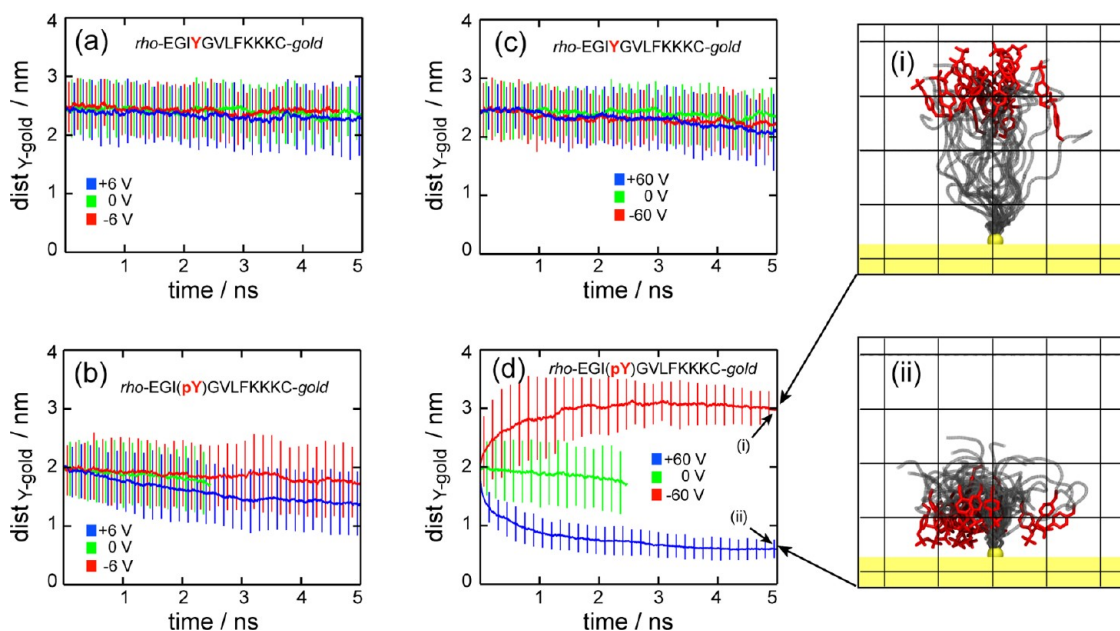


Figure 5. Bending and stretching of phosphorylated peptides revealed by MD simulations. (a–d) Average tyrosine–gold distance of 25 peptides tethered to a planar gold surface. Error bars represent \pm standard deviation. Non-phosphorylated peptide sensor under 0, \pm 6 V bias (a) and under 0, \pm 60 V bias (c). Phosphorylated peptide sensor under 0, \pm 6 V bias (b) and under 0, \pm 60 V bias (d). Panels (i) and (ii) show snapshots of peptide conformations after 5 ns for -60 V (i) and $+60$ V (ii) biases. The peptides are colored in gray, and tyrosine residues in red. Rhodamine residues are not shown. The 25 peptides were aligned using the attaching gold atom, shown in yellow. Grid spacing is 1 nm.

valuable qualitative description of the peptide dynamics experienced by the real device.^{30,38–40}

We simulated two systems, each system composed of 25 peptides, the peptide sequence being the same as in the experiments. The C-terminus was attached to the gold surface, while the N-terminus was linked to a *rho* molecule. The sole difference between the two systems simulated is the phosphorylation of the tyrosine residue at position 4 (details are described in Methods). We applied external electric fields and monitored the conformation of the peptides. Initially, ± 6 V voltage biases were applied. Figures 5a,b show the average distance between the planar surface and the phenol oxygen of tyrosine for non-phosphorylated and phosphorylated sequences. The non-phosphorylated peptides are insensitive to the applied biases. For the phosphorylated peptides, we observed a small response for different voltage polarities. In order to speed up the response we increased the bias to ± 60 V. In an additional calculation (see Figure 2c,d), we established the electric field around an actual GNP-coated nanocone surface, expecting that the field is not spatially homogeneous. We found that the electrostatic field focuses near the surface of the GNPs, giving rise to a high-field gradient near the peptides, the value of which corresponds roughly to the field arising near a flat model surface at ± 60 V biases. This result suggests that the high bias assumed in the simulation may actually reflect values near the tethered peptides.

Figure 5c,d show the distance between tyrosine and gold surface for ± 60 V biases for non-phosphorylated

and phosphorylated sequences. For non-phosphorylated peptides, the results for ± 60 V (Figure 5c) are similar to the results for ± 6 V (Figure 5a); that is, the degree of peptide stretching is not affected by the applied field. Conversely, conformations of phosphorylated peptides depend on the voltage polarity. It is evident from Figure 5d that tyrosine–gold distances converged to either complete stretching (-60 V, red line) or complete bending ($+60$ V, blue line) values. Figure 5i and ii present snapshots of the final conformation after 5 ns of MD simulations. The negative charge of phosphorylated tyrosine influenced the peptide conformation, inducing stretching for negative voltages (Figure 5i) and coiling for positive ones (Figure 5ii). A movie showing dynamic bending and stretching of the phosphorylated peptides is provided in the Supporting Information.

MD simulations confirmed the key interpretation of SERS spectra given above, namely, that phosphorylated peptides change their conformations under applied electric fields, while non-phosphorylated peptides remain insensitive to such fields. The MD results suggest, therefore, that the peptide-conjugated nanosurface we created is an ideal electrophotonic molecular conformation sensor to detect phosphorylation and, thus, capture protein kinase activity.

The MD simulations revealed also possible impediments to sensor performance; this information can be used to optimize sensor characteristics. First, we observed in all simulations aggregation of *rho* residues into dimers and trimers (Figure 6a). Even though

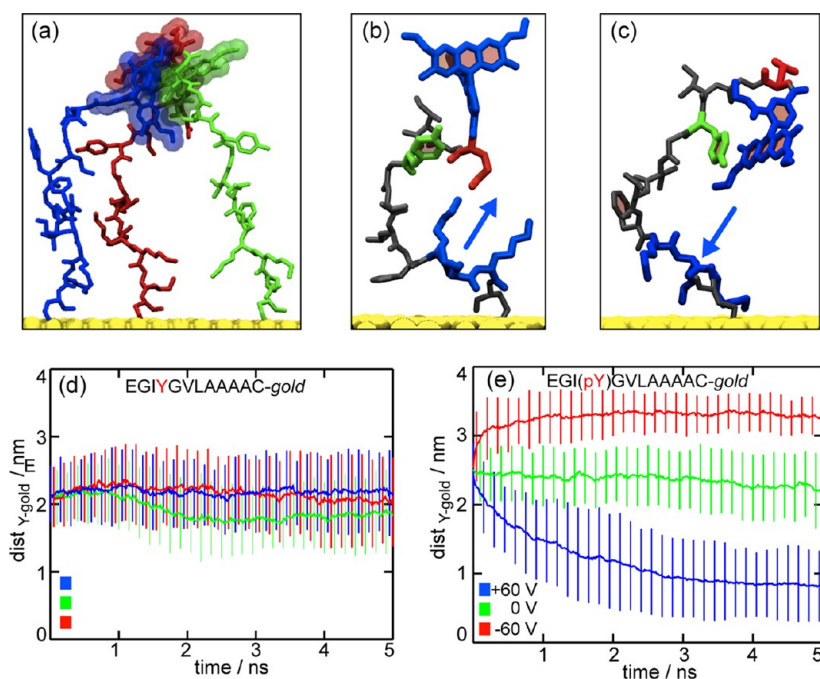


Figure 6. Characteristics of initial and optimized sequences revealed by MD simulations. (a) Aggregation of three *rho* residues of non-phosphorylated peptides at 0 V. Aggregation of *rho* was observed in all MD simulations of the initial sequence. (b, c) Orientation of lysine residues of a non-phosphorylated peptide under +60 V and -60 V biases, respectively. Positively charged lysine residues respond to the external electric field; blue arrows highlight lysine direction. Positively charged residues are colored in blue, tyrosine in green, and negatively charged residues in red. (d, e) Response of the proposed new sequence (EGIYGVLAAAAC) to 0, ± 60 V. The non-phosphorylated new sequence is insensitive to an electric field (d) and, when phosphorylated, is highly responsive to an external electric field (e). Error bars represent \pm standard deviation.

clotting of *rho* does not affect peptide stretching, it does reduce the accessibility of tyrosine residues, which is of critical importance for a functional device. Second, simulations showed that the three lysines at positions 9 to 11 (see Figure 6b,c) are actually not required in our device; in microfluidic electrophoresis uses of the peptides, these positively charged lysines drive the non-phosphorylated peptides in the opposite direction from the negatively charged phosphorylated ones.²⁵

The MD results suggested then two improvements of the peptide used. First, the *rho* residues should be removed to avoid aggregation. Fortunately, rhodamine end groups are not required, as the spectroscopic signal depends on SERS and not on metal-enhanced fluorescence. Second, the lysine residues should be replaced by small, noncharged residues, as the aliphatic lysine tails adhere to the gold surface as well as to other peptide residues. Accordingly, we propose, based on the MD results, the modified sequence EGIYGVLAAAAC, which preserves the active sequence positions 1 to 7 (EGIYGVL), removes *rho*, replaces lysines with alanines, the later one being small residues that do not bind gold,⁴¹ and replaces phenylalanine at position 8 by alanine. The proposed sequence was tested using MD simulations at ± 60 V. The simulated response is optimal: non-phosphorylated peptides are insensitive to voltage biases (Figure 6d); phosphorylated peptides respond sensitively to voltage polarity

(Figure 6e). The suggested sequence still needs to be bench-tested for SERS, but if it were successful, it would overcome shortcomings of the initial design.

CONCLUSIONS

We studied the electrostatic interaction between surface-tethered peptides and a metallic nanosurface. By altering the surface charge polarity and electrostatic field near the surface, we were able to induce peptide conformational changes, *i.e.*, stretching or coiling. The sub-nanometer conformational change was greatly amplified and measured by a distance-dependent near-field optical detection method, surface-enhanced Raman spectroscopy. This method was shown to also clearly identify the phosphorylation state of the peptide probes through SERS signal variations upon application of different polarized electric fields. The method is sensitive enough to permit reliable identification of other charge-related biomolecule conformations on metallic nanosurfaces. The peptide–surface interactions underlying the method were elucidated at the atomic level by MD simulations, which support the interpretation of our SERS spectroscopy results. MD simulations also suggest a new peptide sequence to further improve the performance of the suggested device. The experimental and simulation results of our study establish a proof-of-concept for novel nanophotonic peptide phosphorylation sensors to be employed for high-throughput, high-sensitivity kinase

profiling. In addition, the demonstrated electro-optical experiment and MD simulation approach should be

widely applicable for the development of molecular level bio–nano interface interactions in general.

METHODS

SERS Substrate Fabrication. The photolithography pattern is created on a polished 4 in. silicon wafer surface with rectangular dies of 18 mm \times 24 mm size; subsequently, the wafer can be diced off, allowing each die to become a sensor attached to a standard 25 mm \times 75 mm biological glass slide. The active area on each sensor is a 5 \times 5 square array of 1.5 mm \times 1.5 mm size. High-density nanocones were formed inside the squares to form an active sensor surface. The method to furnish nanocones, simultaneous plasma-enhanced reactive ion synthesis and etching (SPERISE), has been introduced in a previous publication.²⁷ Finally, 5 nm titanium and then 80 nm gold were deposited on top of the nanocone structures using e-beam evaporation to obtain the plasmonic property needed for spectroscopic enhancement. Instead of producing a single coating, the gold atoms tend to aggregate to isolated gold nanoparticles of 5 to 50 nm diameter (Figure 2b); the GNPs spread regularly around the entire nanocone tip and sidewall, allowing the sensor to exhibit uniform spatial detection.

Peptides and Rhodamine Samples. Two sets of synthetic peptides were employed: *rho*-EGI(Y)GVLFKKKC and *rho*-EGI(pY)GVLFKKKC. Both sets of peptides contain N-terminal-bound rhodamine 6G fluorophores. All peptides were obtained as >95% purified samples. The peptide solution at 1 μ M concentration was prepared in water with DMSO or other agents and mixed with a small amount of dithiothreitol. *Rho* solutions in the concentration range 1 pM to 100 μ M were prepared by serial dilution of a measured amount of *rho* powder purchased from Sigma-Aldrich Corporation.

Immobilizing Peptide Probes. The peptide probes were immobilized on the gold-coated SERS substrate surface *via* gold–thiol bonds formed between their C-terminal cysteine and gold atoms. Droplets of 1.5 μ L of phosphorylated and non-phosphorylated peptide solution were separately spotted on the substrate surface. A small amount of dithiothreitol (Sigma Aldrich) was added into the peptide solutions to prevent disulfide bond formation between two peptides. To ensure the peptide bonding, the substrate was sealed in a Petri dish and incubated at 310 K and 100% humidity for about 24 h. After incubation, the substrate was thoroughly washed and cleaned with distilled water to ensure that all free peptides and other agents were completely removed from the surface.

SERS Measurement. All SERS spectra were taken with a sample-scanning Raman spectrometer system as described earlier.³⁴ The system comprised a semiconductor 785 nm CW diode laser, a microscopy system, a 3D scanning stage, and a thermoelectric-cooled (183 K) CCD camera (PIXIS-400, Princeton Instruments). The spectral resolution was approximately 1.5 cm^{-1} in the near-infrared range. A 10 \times microscope objective lens (Mitutoyo infinity-corrected long working distance objectives) with an effective focal length of 20 mm and diameter of 24 mm was used to focus the excitation laser beam onto the sample and to collect the backscattered radiation.

Atomic Level Models. The atomic level systems modeled in MD simulations were composed of the gold surface, 25 peptides, water, and ions and comprised about 111 000 atoms. The gold surface assumed corresponds to a face-centered cubic (fcc) gold slab of 10.2 nm \times 10.2 nm horizontal area and 2.5 nm height, exposing the {100} crystal face to the solvent. The peptide sequences were attached to the gold surface through their cysteine group *via* a S–Au covalent bond. The starting conformation of the peptides was random coil; that is, there was no defined initial secondary structure. Twenty-five peptides were attached to the gold surface, conforming to a 2 nm \times 2 nm square grid. The final peptide concentration was about 2.4 peptides nm^{-2} , the concentration expected for a 1 μ M solution, as employed in the experiments. After attaching the peptides to the surface,

the system was solvated using a 9 nm \times 9 nm water box; to neutralize the system, either Na^+ or Cl^- ions were added.

Force Field Parameters. The force field parameters for peptides and ions were taken from the CHARMM force field,^{42–44} and the TIP3P model was used for water.⁴⁵ Gold parameters were adopted from two references: bonding terms involving gold and cysteine were taken from Bizzarri *et al.*,⁴⁶ namely, bond (Au–S), angle (Au–S–C), and dihedral (Au–S–C–C) terms; nonbonding terms for gold surface atoms were taken from Heinz *et al.*,⁴⁷ the latter terms accurately reproducing, through a Lennard-Jones potential, the interface properties of fcc crystals. Rhodamine parameters were taken from Vaiana *et al.*⁴⁸ The peptide bond between *rho* and the N-terminus of the peptides was described by homology using model compounds from the CHARMM force field.

MD Protocols. MD simulations were carried out using the program NAMD 2.7.³⁶ Detailed MD protocols are described elsewhere^{36,37} and briefly summarized below. Simulations were performed assuming periodic boundary conditions, a 1 fs time step, the particle-mesh-Ewald method for long-range electrostatics and van der Waals interactions with a cutoff of 12 Å, and a switching function starting at 10 Å. Temperature was maintained at 300 K using a Langevin thermostat. For MD simulations performed in the NpT ensemble, a hybrid Nosé-Hoover Langevin piston was used to maintain pressure at 1 atm.

The systems were equilibrated as follows: Systems were minimized for 2000 steps and then equilibrated in the NpT ensemble for 3 ns with the gold, peptides, and rhodamine structures constrained using harmonic forces with a spring constant of 10 $\text{kcal mol}^{-1} \text{Å}^{-2}$. Subsequently, constraints were applied only to the gold structure, and the systems were equilibrated for 1 ns in the NpT ensemble, followed by 1 ns of simulation in the NVT ensemble. The last frames of the MD equilibrations were used as starting structures for voltage-biased simulations under NVT conditions. Voltage biases were applied along the *z*-axis chosen normal to the gold surface. A positive voltage induces cations to move upward, *i.e.*, in the +*z* direction.

Conflict of Interest: The authors declare no competing financial interest.

Acknowledgment. We thank X. Zou for helpful discussions and J. Lu for advice on graphics. This work was supported by grants from NIH (P41-RR05969), NSF (CBET-0708459, PHY0822613), and the University of Illinois at Urbana–Champaign and by an NIH/NCI SCCNE Nanotechnology Grant. We acknowledge supercomputer time provided by the Pittsburgh Supercomputing Center and the National Center for Supercomputing Applications *via* Large Resources Allocation Committee grant MCA93S028 and by the Turing Xserve Cluster of the University of Illinois at Urbana–Champaign.

Supporting Information Available: Figure showing a schematic view of the experimental SERS measurement system, a table listing quantitative SERS band assignments corresponding to peak frequencies stated in Figure 3b, and a movie of the simulated response of peptides to different voltage polarities. This material is available free of charge *via* the Internet at <http://pubs.acs.org>.

REFERENCES AND NOTES

- Huang, Z.; Boulatov, R. Chemomechanics: Chemical Kinetics for Multiscale Phenomena. *Chem. Soc. Rev.* **2011**, *40*, 2359–2384.
- Tashiro, R.; Sugiyama, H. Biomolecule-Based Switching Devices That Respond Inversely to Thermal Stimuli. *J. Am. Chem. Soc.* **2005**, *127*, 2094–2097.

3. Saha, S.; Stoddart, J. F. Photo-Driven Molecular Devices. *Chem. Soc. Rev.* **2007**, *36*, 77–92.
4. Heath, J. R. Molecular Electronics. *Annu. Rev. Mater. Res.* **2009**, *39*, 1–23.
5. Ariga, K.; Mori, T.; Hill, J. P. Control of Nano/Molecular Systems by Application of Macroscopic Mechanical Stimuli. *Chem. Sci.* **2011**, *2*, 195–203.
6. Duriska, M. B.; Neville, S. M.; Moubaraki, B.; Cashion, J. D.; Halder, G. J.; Chapman, K. W.; Balde, C.; Létard, J.-F.; Murray, K. S.; Kepert, C. J.; *et al.* A Nanoscale Molecular Switch Triggered by Thermal, Light, and Guest Perturbation. *Angew. Chem.* **2009**, *121*, 2587–2590.
7. Browne, W. R.; Feringa, B. L. Light Switching of Molecules on Surfaces. *Annu. Rev. Phys. Chem.* **2009**, *60*, 407–428.
8. Joachim, C.; Gimzewski, J. K.; Aviram, A. Electronics Using Hybrid-Molecular and Mono-Molecular Devices. *Nature* **2000**, *408*, 541–548.
9. Kang, T.; Hong, S.; Choi, I.; Sung, J. J.; Kim, Y.; Hahn, J.-S.; Yi, J. Reversible pH-Driven Conformational Switching of Tethered Superoxide Dismutase with Gold Nanoparticle Enhanced Surface Plasmon Resonance Spectroscopy. *J. Am. Chem. Soc.* **2006**, *128*, 12870–12878.
10. Crescenzi, O.; Tomaselli, S.; Guerrini, R.; Salvadori, S.; D'Ursi, A. M.; Temussi, P. A.; Picone, D. Solution Structure of the Alzheimer Amyloid β -Peptide (1–42) in An Apolar Micro-environment. *Eur. J. Biochem.* **2002**, *269*, 5642–5648.
11. Latz, E.; Verma, A.; Visintin, A.; Gong, M.; Sirois, C. M.; Klein, D. C. G.; Monks, B. G.; McKnight, C. J.; Lamphier, M. S.; Duprex, W. P.; *et al.* Ligand-Induced Conformational Changes Allosterically Activate Toll-Like Receptor 9. *Nat. Immunol.* **2007**, *8*, 772–779.
12. Anker, J. N.; Hall, W. P.; Lyandres, O.; Shah, N. C.; Zhao, J.; Van Duyne, R. P. Biosensing with Plasmonic Nanosensors. *Nat. Mater.* **2008**, *7*, 442–453.
13. Chou, I. H.; Benford, M.; Beier, H. T.; Coté, G. L.; Wang, M.; Jing, N.; Kameoka, J.; Good, T. A. Nanofluidic Biosensing for β -Amyloid Detection Using Surface Enhanced Raman Spectroscopy. *Nano Lett.* **2008**, *8*, 1729–1735.
14. Love, J. C.; Estroff, L. A.; Kriebel, J. K.; Nuzzo, R. G.; Whitesides, G. M. Self-Assembled Monolayers of Thiolates on Metals as a Form of Nanotechnology. *Chem. Rev.* **2005**, *105*, 1103–1169.
15. Sallinen, S.-L.; Sallinen, P. K.; Haapasalo, H. K.; Helin, H. J.; Helén, P. T.; Schraml, P.; Kallioniemi, O.-P.; Kononen, J. Identification of Differentially Expressed Genes in Human Gliomas by DNA Microarray and Tissue Chip Techniques. *Cancer Res.* **2000**, *60*, 6617–6622.
16. Phizicky, E.; Bastiaens, P. I. H.; Zhu, H.; Snyder, M.; Fields, S. Protein Analysis on a Proteomic Scale. *Nature* **2003**, *422*, 208–215.
17. Endo, T.; Kerman, K.; Nagatani, N.; Hiepa, H. M.; Kim, D.-K.; Yonezawa, Y.; Nakano, K.; Tamiya, E. Multiple Label-Free Detection of Antigen-Antibody Reaction Using Localized Surface Plasmon Resonance-Based Core-Shell Structured Nanoparticle Layer Nanochip. *Anal. Chem.* **2006**, *78*, 6465–6475.
18. Eggeling, C.; Fries, J. R.; Brand, L.; Günther, R.; Seidel, C. A. M. Monitoring Conformational Dynamics of a Single Molecule by Selective Fluorescence Spectroscopy. *Proc. Natl. Acad. Sci. U. S. A.* **1998**, *95*, 1556–1561.
19. Krimm, S.; Bandekar, J. Vibrational Spectroscopy and Conformation of Peptides, Polypeptides, and Proteins. *Adv. Protein Chem.* **1986**, *38*, 181–364.
20. Wishart, D. S.; Sykes, B. D.; Richards, F. M. Relationship between Nuclear Magnetic Resonance Chemical Shift and Protein Secondary Structure. *J. Mol. Biol.* **1991**, *222*, 311–333.
21. Bialik, S.; Kimchi, A. The Death-Associated Protein Kinases: Structure, Function, and Beyond. *Annu. Rev. Biochem.* **2006**, *75*, 189–210.
22. Kennedy, B. J.; Spaeth, S.; Dickey, M.; Carron, K. T. Determination of the Distance Dependence and Experimental Effects for Modified SERS Substrates Based on Self-Assembled Monolayers Formed Using Alkanethiols. *J. Phys. Chem. B* **1999**, *103*, 3640–3646.
23. Gartia, M. R.; Bond, T. C.; Liu, G. L. Metal-Molecule Schottky Junction Effects in Surface Enhanced Raman Scattering. *J. Phys. Chem. A* **2011**, *115*, 318–328.
24. Albrecht, M. G.; Creighton, J. A. Anomalous Intense Raman Spectra of Pyridine at a Silver Electrode. *J. Am. Chem. Soc.* **1977**, *99*, 5215–5217.
25. Caliper Life Sciences. <http://www.caliperls.com/> (accessed Jul 10, 2012).
26. Zhu, K.; Zhao, J.; Lubman, D. M.; Miller, F. R.; Barder, T. J. Protein *pI* Shifts due to Posttranslational Modifications in the Separation and Characterization of Proteins. *Anal. Chem.* **2005**, *77*, 2745–2755.
27. Chen, Y.; Xu, Z.; Gartia, M. R.; Whitlock, D.; Lian, Y.; Liu, G. L. Ultrahigh Throughput Silicon Nanomanufacturing by Simultaneous Reactive Ion Synthesis and Etching. *ACS Nano* **2011**, *5*, 8002–8012.
28. Oh, Y.-J.; Jeong, K.-H. Glass Nanopillar Arrays with Nanogap-Rich Silver Nanoislands for Highly Intense Surface Enhanced Raman Scattering. *Adv. Mater.* **2012**, *24*, 2234–2237.
29. Xu, Z.; Chen, Y.; Gartia, M. R.; Jiang, J.; Liu, G. L. Surface Plasmon Enhanced Broadband Spectrophotometry on Black Silver Substrates. *Appl. Phys. Lett.* **2011**, *98*, 241904-1–241904-3.
30. Lee, E. H.; Hsin, J.; Sotomayor, M.; Comellas, G.; Schulten, K. Discovery Through the Computational Microscope. *Structure* **2009**, *17*, 1295–1306.
31. Brolo, A. G.; Irish, D. E.; Szymanski, G.; Lipkowski, J. Relationship between SERS Intensity and Both Surface Coverage and Morphology for Pyrazine Adsorbed on a Polycrystalline Gold Electrode. *Langmuir* **1998**, *14*, 517–527.
32. Houseman, B. T.; Huh, J. H.; Kron, S. J.; Mrksich, M. Peptide Chips for the Quantitative Evaluation of Protein Kinase Activity. *Nat. Biotechnol.* **2002**, *20*, 270–274.
33. Chen, Y.; Xu, Z.; Liu, G. L.; Coppé, J.-P. Highly Sensitive Surface-Enhanced Raman Nano-Probing for Direct Proteomic Profiling. *IEEE Sens. 2010* **2010**, 2295–2298.
34. Coppé, J.-P.; Xu, Z.; Chen, Y.; Liu, G. L. Metallic Nanocone Array Photonic Substrate for High-Uniformity Surface Deposition and Optical Detection of Small Molecules. *Nanotechnology* **2011**, *22*, 245710.
35. Jeanmaire, D. L.; Van Duyne, R. P. Surface Raman Spectroelectrochemistry: Part I. Heterocyclic, Aromatic, and Aliphatic Amines Adsorbed on the Anodized Silver Electrode. *J. Electroanal. Chem. Interfacial Electrochem.* **1977**, *84*, 1–20.
36. Phillips, J. C.; Braun, R.; Wang, W.; Gumbart, J.; Tajkhorshid, E.; Villa, E.; Chipot, C.; Skeel, R. D.; Kálc, L.; Schulten, K. Scalable Molecular Dynamics with NAMD. *J. Comput. Chem.* **2005**, *26*, 1781–1802.
37. Cruz-Chu, E. R.; Aksimentiev, A.; Schulten, K. Ionic Current Rectification through Silica Nanopores. *J. Phys. Chem. C* **2009**, *113*, 1850–1862.
38. Braun, R.; Sarikaya, M.; Schulten, K. Genetically Engineered Gold-Binding Polypeptides: Structure Prediction and Molecular Dynamics. *J. Biomater. Sci., Polym. Ed.* **2002**, *13*, 747–757.
39. Lu, D.; Aksimentiev, A.; Shih, A. Y.; Cruz-Chu, E. R.; Freddolino, P. L.; Arkhipov, A.; Schulten, K. The Role of Molecular Modeling in Bionanotechnology. *Phys. Biol.* **2006**, *3*, S40–S53.
40. Aksimentiev, A.; Brunner, R.; Cohen, J.; Comer, J.; Cruz-Chu, E. R.; Hardy, D.; Rajan, A.; Shih, A.; Sigalov, G.; Yin, Y.; *et al.* Computer Modeling in Biotechnology: A Partner in Development. In *Nanostructure Design: Methods and Protocols*; Gazit, E., Nussinov, R., Eds.; Methods in Molecular Biology; Humana Press: New York, 2008; Vol. 474, pp 181–234.
41. Willett, R. L.; Baldwin, K. W.; West, K. W.; Pfeiffer, L. N. Differential Adhesion of Amino Acids to Inorganic Surfaces. *Proc. Natl. Acad. Sci. U. S. A.* **2005**, *102*, 7817–7822.
42. MacKerell, A. D., Jr.; Bashford, D.; Bellott, M.; Dunbrack, R. L., Jr.; Evanseck, J. D.; Field, M. J.; Fischer, S.; Gao, J.; Guo, H.; Ha, S.; *et al.* All-Atom Empirical Potential for Molecular Modeling and Dynamics Studies of Proteins. *J. Phys. Chem. B* **1998**, *102*, 3586–3616.

43. MacKerell, A. D., Jr. Empirical Force Fields for Biological Macromolecules: Overview and Issues. *J. Comput. Chem.* **2004**, *25*, 1584–1604.
44. Buck, M.; Bouguet-Bonnet, S.; Pastor, R. W.; MacKerell, A. D., Jr. Importance of the CMAP Correction to the CHARMM22 Protein Force Field: Dynamics of Hen Lysozyme. *Biophys. J.* **2006**, *90*, L36–L38.
45. Jorgensen, W. L.; Chandrasekhar, J.; Madura, J. D.; Impey, R. W.; Klein, M. L. Comparison of Simple Potential Functions for Simulating Liquid Water. *J. Chem. Phys.* **1983**, *79*, 926–935.
46. Bizzarri, A. R.; Costantini, G.; Cannistraro, S. MD Simulation of a Plastocyanin Mutant Adsorbed onto a Gold Surface. *Biophys. Chem.* **2003**, *106*, 111–123.
47. Heinz, H.; Vaia, R. A.; Farmer, B. L.; Naik, R. R. Accurate Simulation of Surfaces and Interfaces of Face-Centered Cubic Metals Using 12–6 and 9–6 Lennard-Jones Potentials. *J. Phys. Chem. C* **2008**, *112*, 17281–17290.
48. Vaiana, A. C.; Schulz, A.; Wolfrum, J.; Sauer, M.; Smith, J. C. Molecular Mechanics Force Field Parameterization of the Fluorescent Probe Rhodamine 6G Using Automated Frequency Matching. *J. Comput. Chem.* **2003**, *24*, 632–639.